Swinburne Research Bank
http://researchbank.swinburne.edu.au

Author:	Thi-Hai-Yen Vu, Weijian Chen, Xiaofan Deng, Cho Fai Jonathan Lau, Shujuan Huang, Anita Ho-Baillie, Baohua Jia, and Xiaoming Wen
Title:	Visualizing the Impact of Light Soaking on Morphological Domains in an Operational Cesium Lead Halide Perovskite Solar Cell
Year:	2020
Journal:	The Journal of Physical Chemistry Letters
Volume:	11
Pages:	136-143
URL:	http://hdl.handle.net/1959.3/453397
Copyright:	This document is the Accepted Manuscript version of a Published Work that appeared in final form in The Journal of Physical Chemistry Letters, copyright © American Chemical Society 2019, after peer review and technical editing by the publisher. To access the final edited and published work see https://doi.org/10.1021/acs.jpclett.9b03210.

This is the author’s version of the work, posted here with the permission of the publisher for your personal use. No further distribution is permitted. You may also be able to access the published version from your library.

The definitive version is available at: https://doi.org/10.1021/acs.jpclett.9b03210

Visualizing the Impact of Light-Soaking on Morphological Domains in an Operational Cesium Lead Halide Perovskite Solar Cell

Thi-Hai-Yen Vu,[†][‡] Weijian Chen,[†][‡] Xiaofan Deng,[§] Cho Fai Jonathan Lau,[§] Shujuan Huang,[§] Anita Ho-Baillie,[§] Baohua Jia,[†]* Xiaoming Wen[†]*

[†] Centre for Translational Atomaterials, Swinburne University of Technology, Hawthorn, Victoria 3122, Australia

[§]Australian Centre for Advanced Photovoltaics, School of Photovoltaic and Renewable Energy Engineering, UNSW Sydney, Sydney 2052, Australia

[‡]These authors contributed equally to this work.

*E-mail: X.W.: xwen@swin.edu.au; B.J.: bjia@swin.edu.au

Abstract:

The dynamics of photogenerated carriers and mobile ions in an operational cesium lead halide (CsPbI3) perovskite solar cells (PSC) under working conditions are studied using nanoscale resolved photoluminescence (PL) lifetime imaging microscopy. The temporally and spatially resolved PL changes in the perovskite film during and after bias light soaking are dynamically monitored. By analyzing the dynamic variations of PL intensity and PL lifetime of an open-circuited PSC, the impacts of light soaking are revealed by a dynamic model of photogenerated charge carrier and mobile ions. We confirmed the different behavior from morphological domains interiors and domains boundaries during light soaking, which shed light on the engineering of the domain interiors in additions to the commonly considered domain boundary strategies. This work provides a full picture of the photogenerated process in an operating PSC and therefore guides the design and operation of perovskite-based optoelectronic devices.

Table of Contents:

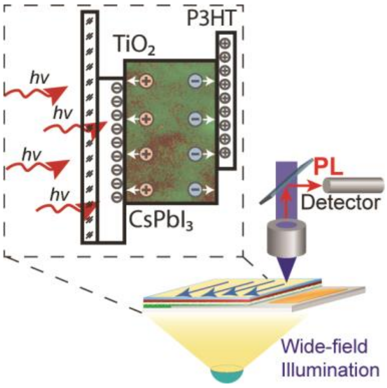

Since the first successful integration of hybrid halide perovskite in solar cells,[1] this class of photovoltaic devices has archived impressive power conversion efficiency exceeding 25% in only a decade.[2] Besides excellent properties in photovoltaics, perovskites have attracted immense attention in the applications of lasers, LED and detectors due to their intriguing optical-electronic properties and low-cost fabrication.[3–5] Perovskites behavior under different situations has been intensively investigated and applied to improve cell performance. It has been a consensus that both combined effects of charge carriers (electron and hole) and mobile ions migration occur in perovskite and determine the device performance. These complicated physical mechanisms, together with the dynamic timescale spanning from nanoseconds to hours and nanoscale micro-processes, seriously impede the physical understanding, especially in working condition, which is the key issue to accelerate commercialization of perovskite-based optoelectronic application.

Carrier dynamics is one of the most principle questions because it is closely relevant to the performance of the devices. Charge carrier extraction, transportation, and collection have crucial implications to photovoltaics device in terms of performance and stability. On the other hand, as hybrid halide perovskites have been confirmed to be mixed electronic-ionic conductors, mobile ions play a critical role in the stability of the devices.[6] The mobile ions, essentially being defects in the lattice, response much slower than that of photogenerated carriers[7], creating complicated behavior, especially under working conditions where light illumination and the bias voltage applied. The effects of light soaking in perovskites have been intensively investigated.[8–15] Xing et al.[16] reported that ion accumulation at the interface could act as recombination traps and inhibit electron and hole transportation. Xiao et al.[17] suggested that switchable photovoltaic effect in perovskite solar cells is related to the drift of ionic vacancies in perovskite.

It is well known that the grain and grain boundary behaves very differently in solution fabricated perovskite solar cells.[18] However, recent reports identify that these "grain" observed by SEM without diffraction information might consist of sub-grains with different crystal orientations identified by electron back-scattered diffraction (EBSD),[19] which is technically inaccurate to be termed as "grains" in crystallography definition. In this context, the term "morphological domain" is specifically referred to the "domain" identified as "grain" in SEM in previous investigation.

Time-resolved PL with spatially resolved microscopy down to micrometer resolution can provide invaluable information for the deep understanding of the device operation.[20,21] In perovskite-based devices, instead of the intrinsic bulk recombinations, the charge carrier extraction, and interface recombination dominate the PL dynamics.[22–24] In previous studies, photoluminescence (PL), fluorescence lifetime imaging microscopy (FLIM) and I-V characterization have been shown to be powerful approaches to determine the quality of perovskites and the performance of perovskite solar cells. [25,26] Mosconi et al.[8] combined PL measurement and computational modeling to explain the light-induced elimination of Frenkel defects in lead iodide perovskite. Zhao et al.[10] employed time-dependent PL to study light soaking effect in bulk perovskite and the interfaces between perovskite and carrier transport layers. They proposed that the decrease of charge accumulation at the interfaces is caused by the filling of generated carriers into surface defects or by ion migration induced internal electric field. However, in addition to PL quenching caused by the electron and hole transport layers in operational solar cells, the high reflection of the gold electrode and bias illumination significantly increase the difficulty for the FLIM measurement.

In this work, we develop a high resolution, high sensitivity fluorescence lifetime imaging spectroscopy (FLIM) to investigate a fully operational perovskite solar cell. We achieve dynamic detection of the operational perovskite solar cells (PSC) under continuous bias light illumination. This method allows the real-time monitoring of microscopic images of PL intensity and PL lifetime. Moreover, it is able to extract the information at specific points or areas, providing a deep insight at perovskites/hole transporting layer interface as well as perovskite morphological domain interiors and domain boundaries. The carrier and mobile ion dynamics in a PSC under working condition are studied, and the impact of bias light illumination and the relevant dark recovery process of the illuminated PSC is revealed.

The $CsPbI_3$ perovskite solar cells used in this study were fabricated with common meso-porous structure as described in previous work, except for dissolving CaI_2.[13] In details, patterned fluorine-doped tin oxide (FTO) coated glass was cleaned in deionized (DI) water with 2% Hellmanex, acetone, and isopropanol, respectively, for 20 minutes by sonication. After drying by N_2 gas, it was treated by UV ozone cleaner for 20 minutes. Subsequently, compact TiO_2 (c-TiO_2) layer was deposited on a clean substrate by spray pyrolysis of titanium dioxide bis(acetylacetonate) in ethanol solution at 450°C then annealed on hot plate at 400°C for 20 minutes. To deposit 100 nm meso-porous TiO_2 (mp-TiO_2), Dyesol 18 NR-T paste diluted in ethanol was spin-coated on c-TiO2 substrate at 4000 rpm for 12 seconds. The substrate was dried at 100°C for 10 min, then annealed at 450 °C for 30 minutes. After cooling, the substrate was cleaned by UVO for 20 minutes and transferred into glovebox for perovskite deposition. CsI and PbI_2 precursors were dissolved in a mixed solution of DMF and DMSO, then the precursor solution was deposit on mp-TiO_2 substrate by gas-assisted spin coating. Formed perovskite film was annealed on a hotplate at 300°C for 10 minutes. Next, hole transport material (HTM) layer was deposited by spin coating 10mg/ml P3HT solution in chlorobenzene at 3000 rpm for 30 s. Finally, a 10 nm thin layer of Au was thermally evaporated on top of the cell. The semi-transparent gold electrode layer allowed the excitation laser to pass through and perovskite PL to be collected while remaining low resistance for normal cell operation. The completed cells were encapsulated from ambient atmosphere and humidity. The complete perovskite solar cells with a structure of glass/FTO/c-TiO_2/mp-TiO_2/$CsPbI_3$ /HTM/gold used in this study is illustrated in Figure 1(a).

To achieve PL image of an operational solar cell, fluorescence lifetime images (FLIM) were acquired by combining time-correlation single photon counting (TCSPC) technique and confocal laser scanning microscopy (MT200, Picoquant), where the setup is presented in Figure 1(b). A bias continuous light (Xenon light with a filter of 400-500 nm, intensity is 72 mW/cm^2) was used to illuminate the sample from glass side, whose intensity was equivalent to 0.72 times of one sun intensity, hereafter referred to as the bias light. An excitation laser beam with a wavelength of 470 nm and repetition rate of 20 MHz was focused onto the perovskite solar cells from the thin gold/HTM side via a 60×/NA1.4 oil immersion objective. The excitation density of the scanning pulsing laser is 200mW/cm^2 and the diameter of the excitation laser spot is estimated to be around 215nm.[27] The PL signal from perovskite was collected from the gold/HTM side via the same objective. The dwelling time at each pixel is set as short as 2 milliseconds, minimizing the impact of the excitation laser on the perovskite while ensuring sufficient exposure and high-quality PL signal. Solar cell performance measurements were conducted via a solar cell I–V testing system with 8Å~8mm^2 aperture, which was calibrated using a reference cell from Abet Technologies Inc. (Class AAA solar simulator) under an illumination power of 100 $mWcm^{-2}$. All J-V measurements were undertaken in ambient temperature.

As a benchmark for monitoring the dynamic variation of an operational solar cell under illumination condition, FLIM scanning images of the pristine perovskite solar cell (PSC) were acquired as shown in Figure 1(c). To avoid un-intentional light exposure, the PSC was kept in the dark chamber before the experiment. Note that in a FLIM image, the brightness/greyscale represents PL intensity and the color scale represents PL lifetime, and the complete scanning time of a 20 μm×20 μm area in Figure 1(c) is 180 s. The morphological domain distributions of the perovskite film are clearly recognizable, with some of the grains show higher PL intensity (brighter pixels) with longer PL lifetime (pixels with green color scale). The general PL intensity and lifetime distribution also indicate that the excitation laser beam only has a negligible impact on the PL properties of the perovskite. Figure 1(d) shows a FLIM image of an identical area when the bias light turning on at time zero T_0. Within the first 30 s of the scanning time, the PL intensity dramatically decreases (darker pixels) with PL lifetime increases (almost all pixels with color turning to green), after which the overall PL intensity across the sample area maintains at low intensities with longer PL lifetime. Moreover, the domain distributions of the perovskite film became indifferentiable, as both brightness and color scale of the whole FLIM image became uniform.

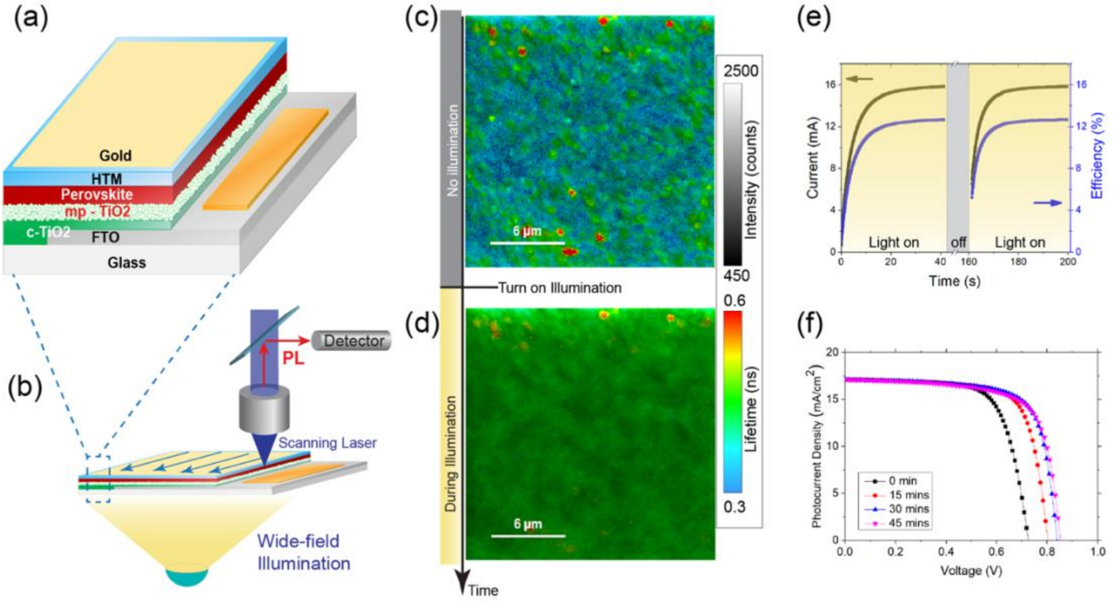

Figure 1. (a) Schematic diagram of perovskite solar cells; (b) schematic diagram of FLIM measurement; FLIM images of perovskite solar cells when the bias light is (c) off and (d) on; (e) photo-current and cell efficiency in relation with light illumination; (f) J-V curves after 0, 15, 30, 45 minutes under light illumination.

The current density and efficiency of the PSC as a function of light soaking time were shown in Figure 1(e). The photocurrent of the PSCs grows from 0 mA within the first 20 s of light soaking time and saturates at a high current of 16 mA. The PSC was kept in dark condition for 120 s after 45 s of initial light soaking, followed by the second round of light soaking for 40 s. The saturated photocurrent (16 mA) and steady-state cell efficiency (12.6%) in the second round of light soaking are the same as the first round, indicating the excellent repeatability. However, the initial photocurrent of the second light soaking experiment is not recorded at 0 mA, but a residue photocurrent of 5 mA and an initial efficiency of 4% was observed (Time = 160 s) of Figure 1(e), and the saturation time is shortened to 10 s after turning on the bias light. Figure 1(f) shows the J-V curves of the PSC with cumulated light soaking times up to 45 minutes. While cumulated light soaking barely increases the short-circuits photocurrent J_{sc} of the PSC, the open-circuit voltage V_{oc} increases from 0.72 V to 0.87 V after 45 minutes of bias light soaking. The correlation of increased V_{oc} and the observed decrease of PL quenching during illumination is discussed in Note 1 of Supporting Information (SI).

Figure 1 shows that while light soaking of PSC has a cumulated effect on increasing open-circuit voltage in a time scale of minutes, the change of PL properties and short-circuit photon-current during light soaking is much quicker, which is within the time scale of seconds. Therefore, by scanning a smaller area with a faster scanning rate, it is feasible to observe the PL properties of each perovskite morphological domains as well as their transformation during and after light-soaking. Figure 2(a-c) show FLIM images of the PSC with an area of 10 μm×10 μm in non-exposure, light-soaking and dark recovery stages, respectively. The scanning time of each FLIM image is 60 s with a dwelling time at each pixel is still two milliseconds. Two consecutive FLIM images of the non-illuminated perovskite are shown in Figure 2(a), which demonstrate exactly the same PL intensity and lifetime with clear morphological domains boundaries and uniform distribution across the whole area. Therefore, it is safe to state that the fast laser scanning excitation does not impact the PL properties of the perovskite film. Figure 2(b) are the FLIM images of the same area during light soaking at selected time frames. After the bias light is turned on, the morphological domains gradually become blurred within a soaking time of 30 s. After 180 s of light soaking, almost all the morphological domains become unrecognizable. With longer light soaking time, the overall color of the FLIM images changes from “blue” to “green”, with some particular parts of the area became “red” after 500s. These changes of FLIM color distribution indicate that the constant increase of effective lifetime over the sample area during light soaking, and the impact of light soaking on perovskite is not uniform across the morphological domains area. Figure 2(c) are the 3 FLIM images of the same area after light soaking, which is the so-called “dark recovery” process. The morphological domains distributions quickly re-appear within a short dark recovery time (~30 s, Figure 2(c), with PL intensity increased and PL lifetime decreased across the whole sample area. However, it takes a much longer time (at least 600 s) to recover back to a state with PL intensity and lifetime comparable to the pristine condition as Figure 2(a). One would raise the question that whether a similar change of perovskite properties can be observed by changing the excitation laser power in the absence of bias light. Please note that the change induced by laser pulse at each pixel will not cumulates to the whole perovskite film as the laser is scanning across the sample area. Therefore, by simply increasing the laser power, changes of properties at the level of operational device will not be observed before damaging the perovskite film.

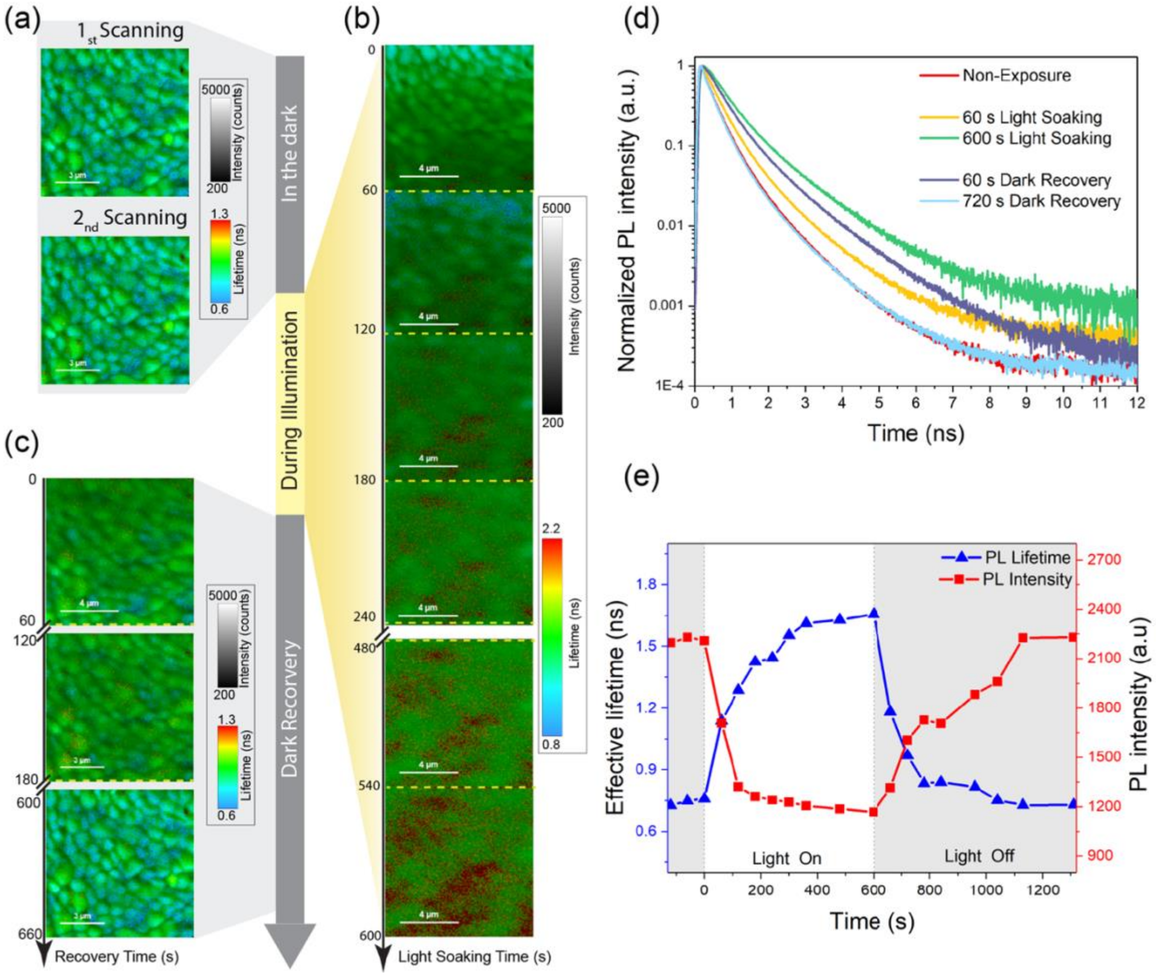

Figure 2. (a) FLIM images of perovskite solar cells (a) before, (b) during and (c) after light illumination; (d) PL decay traces in different illumination conditions; (e) PL Intensity and PL effective lifetime as a function of time.

To quantitively study the light soaking and dark recovery processes, the time-resolved PL decay traces at different time stages are extracted, as shown in Figure 2(d). The PL decay traces can be well fitted using a bi-exponential function $I(t) = A_1 \exp(-t/\tau_1) + A_2 \exp(-t/\tau_2)$ with effective decay lifetimes given by $\tau_{eff} = (A_1\tau_1 + A_2\tau_2)/(A_1 + A_2)$.[28] Figure 2(e) shows the traces of PL intensity and PL lifetime as a function of time, where light soaking time is t=0 to 600 s and dark recovery time is t= 600 s to 1200 s. It is worth noting that: (1) the decrease of PL intensity during light soaking is accompanied by the increase of PL lifetime, while the dark recovery is the reverse process of light soaking; (2) the impact of light soaking is fully recoverable; (3) For both light soaking and dark recovery, majority of the PL intensity and lifetime changes happened within the initial 100 s after turning the bias light on/off, followed by a slow shifting (across the following 500 s). Such PL quenching induced by light soaking within a timescale of minutes have been previously reported in similar perovskite films and ascribed to the light-activated mobile ions,[7,29] and several methods of binding mobile ions are demonstrated to be effective to maintain the high quantum efficiency and thus increase the overall solar cell efficiency.[30,31] However, the impact of light-induced PL quenching varies as perovskite composition changes[32], and also depends on the power density of illumination light.[33]

To investigate the origin of perovskite morphological domains blurring phenomena during light soaking and its dark recovery, the nanoscale spatial distribution of PL intensity across morphological domain boundaries are shown in Figure 3(a) under consecutive light soaking and dark recovery conditions. Figure 3(b) shows the corresponding boxplots of the PL intensity. It is found that there is a significant difference in PL change between the domain boundaries and domains interiors: no noticeable change of PL intensity are observed at domains boundaries during and after light soaking. On the contrary, the PL intensity of the domain interior decreases notably during light soaking. The PL intensity of domain interior after 60 s light soaking (blue curve) is only 50% of that without exposure to the light (red curve). After 540 s of light soaking (yellow curve), the PL intensity of the domain interiors further resuces and become comparable to PL intensity at domain boundaries, which results in that the domains become completely unrecognizable in a FLIM image (i.e. the last FLIM image in Figure 2(b), due to drastically decreased contrast. Moreover, the domain interior accounts for most of PL intensity increase during the dark recovery. These observations confirm that the light soaking effect and its recoveries on perovskite PL changes mostly originate from domain interior, while the domain boundaries, where a larger amount of non-radiative defects reside, are barely responsive to the bias light.

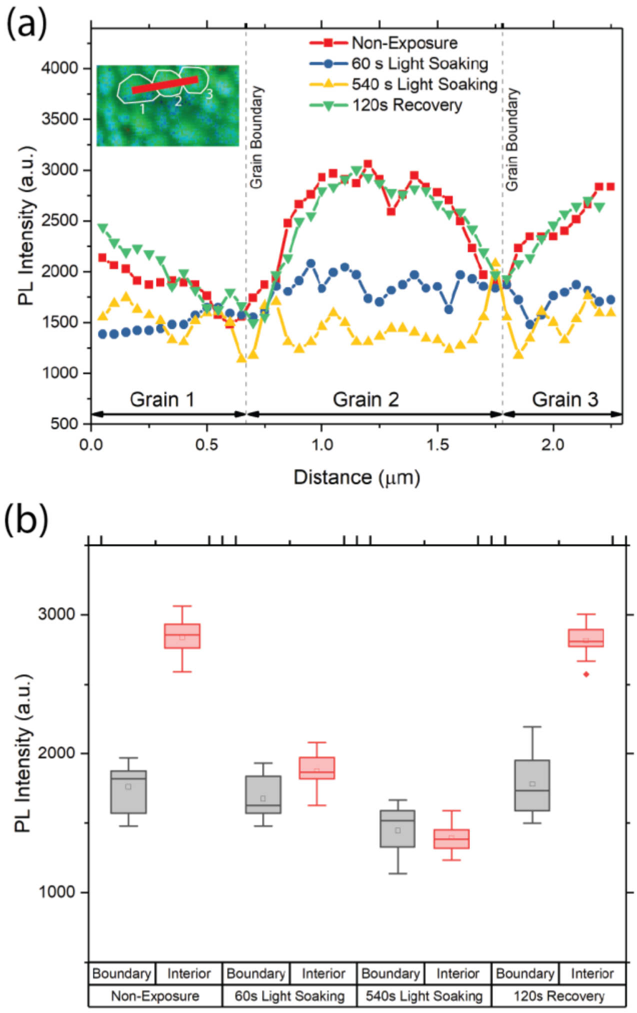

Figure 3. (a) PL intensity as a function of distance across perovskite grains. The inset shows measurement traces (red bars) across three consecutive domains (white circles); (b) boxplot of PL intensity at domain boundary and domain interior distribution under difference illuminating condition.

The above-mentioned FLIM observations demonstrate the impact of light soaking on the carrier dynamics in an operating perovskite solar cell, as well as the corresponding variations of device performance. Essentially, the charge carrier dynamics occur in the nanosecond timescale, which includes (1) Shockley-Read-Hall recombination, (2) electron-hole recombination and (3) carrier extractions by the electron transport layer and hole transport layer for an operational solar cell.[34,35] An effective carrier transport is prerequisite for high-efficiency solar cell. Therefore, a much shorter PL lifetime is usually observed when active layers (perovskite) are covered by a hole transport layer, which is dictated by charge-carriers extraction.[20,36] On the other hand, the slow response in macroscopic time (milliseconds to hours) has been attributed to the activation, migration, accumulation, and depletion of mobile ions,[37,38] specifically including both iodide interstitials ion (I^-) and halide vacancies (V_I^+), due to their low activation energy (hundreds of meV)[8,39,40] and high mobility.[23,41,42] The mobile ions migration timescale is consistent with the observation of PL changes appeared under bias light soaking here and in the literature.[43] Moreover, it has been a consensus that the mobile ion distribution in the active layer of perovskite and interfaces will significantly impact the charge carrier dynamics. During these light soaking and dark recovery processes, there are interactions between charge carriers and mobile ions through Coulomb interaction, which is detectable by monitoring the PL intensity and PL lifetime.

Taking into account the combined effect of charge carrier and mobile ions, we proposed a dynamic model in the $CsPbI_3$ PSC to explain the consecutive observation of PSC performance before, during and after light soaking, as schematically illustrated in

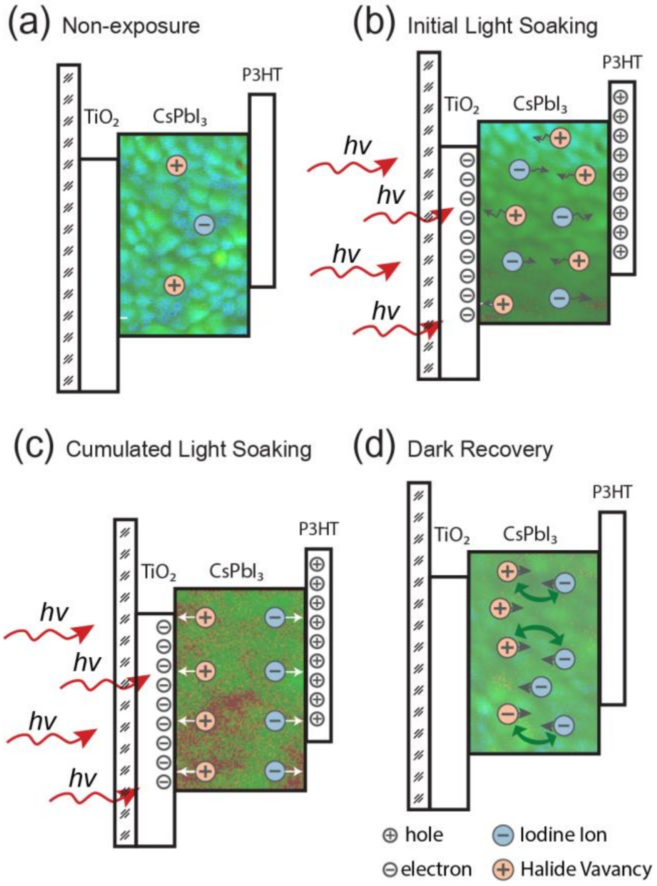

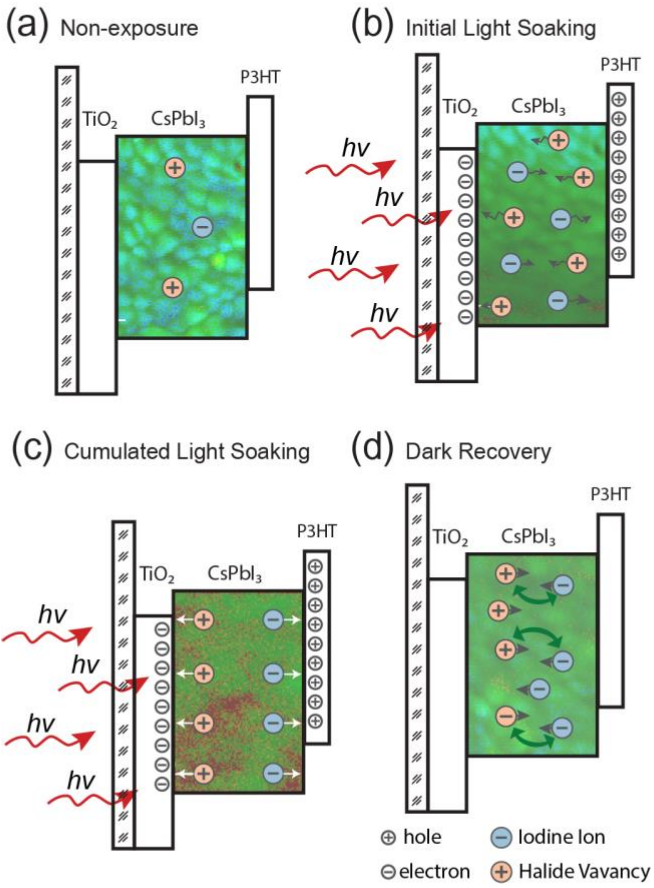

Figure 4. In initial dark condition (

Figure 4(a)), the perovskite in the PSC maintains its as-fabricated electronic properties with a low density of ions. Note here the laser for FLIM imaging has a negligible effect on the charge carrier dynamics, therefore the observed PL is essentially the working properties of the PSC at pristine condition.

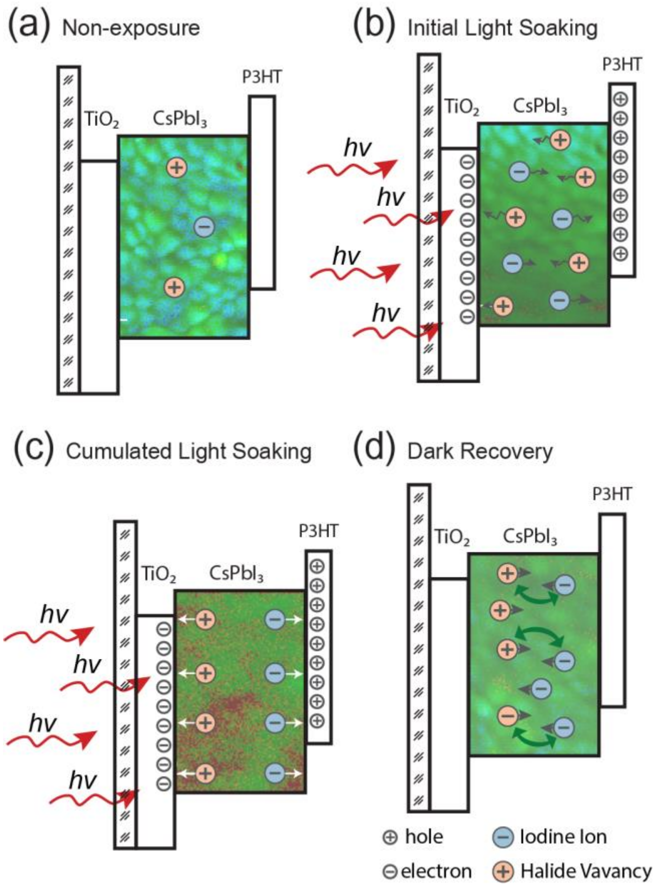

Once bias light (wide-field) illuminates an open-circuited PSC (Figure 4(b)), the photogenerated electrons and holes are effectively transferred/extracted into the electron transporting layer (ETL) and hole transporting layer (HTL), respectively, which produces an internal electric field across the solar cell within a timescale of nanoseconds.[44] With continuous illumination, large number of phonons are generated in the perovskite lattice because the hot carriers photogenerated by the high energy photons can effectively emit the extra energy and relax to the conduction band edge.[45] These phonons couple with the atoms in the lattice and result in the activation of mobile ions in the perovskite, most likely including both I^- and V_{I^+}.[46] While the phonon coupling is within ultrafast timescale(fs-ps), the impact of mobile ions is to take effect via a cumulated timeframe (in terms of seconds). Such an impact of cumulated mobile ions in the timescale of seconds is more pronounced in the case of light-induced phase segregation in mixed halide perovskite which is also found to be related to phonon-electron coupling and lattice distortion on activation of mobile ions.[42,47,48] The emergence of these mobile ions increases the nanometer-scale local electric field, which partly screens the internal electric field generated by the photogenerated charge carriers. On the other hand, it has been shown that such mobile ions will quench the radiative recombination of electron and hole locally, thus macroscopically decreasing PL intensity (Figure 2(e)). Meanwhile, PL lifetime of the perovskite, dictated by hole extraction rate to HTL, is increased. This is ascribed to the hole extraction from perovskite layer becomes slower due to an enhanced energy barrier at the interface during light soaking. It has been confirmed that perovskites are mixed electronic-ionic conductors; and thus the overall current can contribute by both charge carriers and mobile ions.[49] . I^- drifted to the HTL side while V_{I^+} migrated to the opposite ETL site with different mobilities. The directional migration of these mobile ions counters the charge carrier current of the PSC, which results in the slow rise of I_{sc} of PSC under light soaking (Time = 0-20 s in Figure 1(e)). The current saturates as the mobile ions establish a stable distribution under illumination, and directional ionic shift terminates. In other words, the observed slow rise of I_{sc} originates from the concurrence of charge carriers' movement and mobile ion migrations. With a longer bias light illumination (Figure 4(c)), the increased ion population near the interfaces creates another electric field, countering/screening the existing internal electric field, which eventually leads to a steady-state internal electric field with the lower overall field strength. The migration of mobile ion under internal electric field and cumulation at the two ends are relatively slow. One might consider the impact of illumination on the change of interface between perovskite and charge carriers transport layers, which have been previously investigated and discussed in Note 2 of SI.

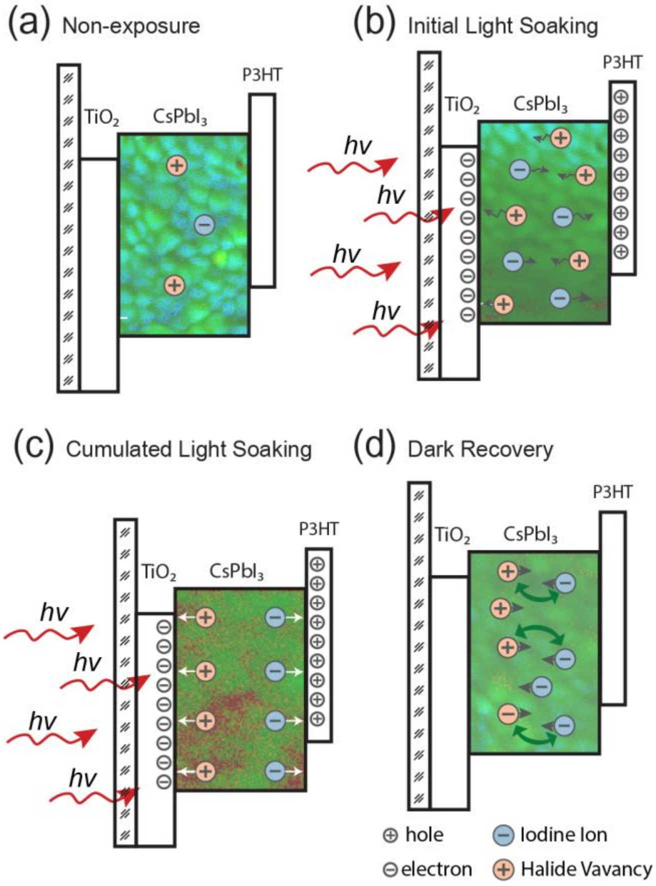

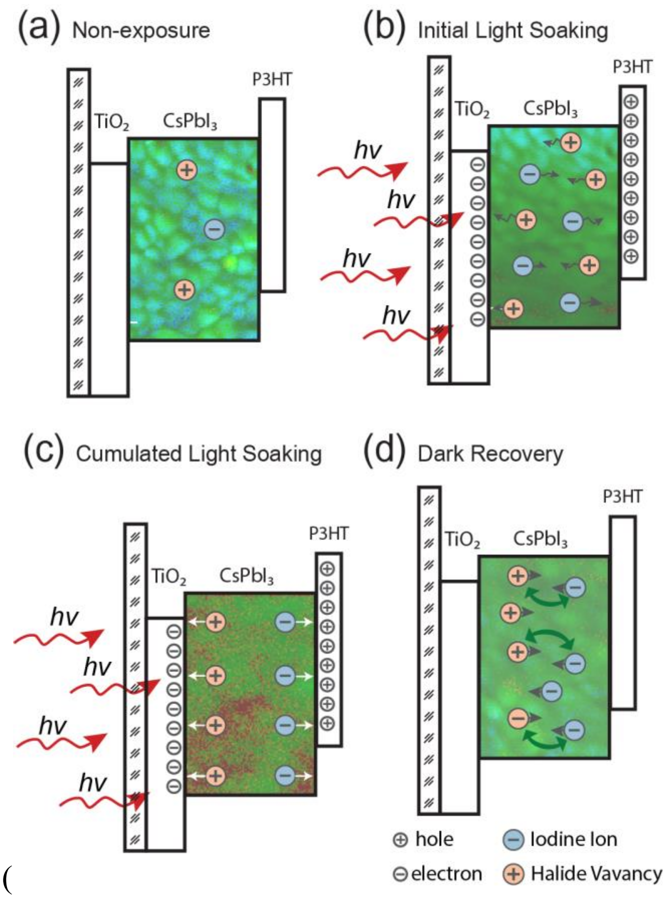

Once the bias light is turned off (Figure 4(d)), the internal electric field induced by bias-light-generated electrons and holes immediately dissipates. With the internal electric field ceases, ion distribution significantly deviates the equilibrium established during light soaking. Driven by such a non-equilibrium, the mobile ions gradually leave the perovskite/transport layer interface. Part of the interstitial and vacancy recombines and results in dissipation, tending to recover the initial equilibrium in the dark. However, migration of the light-activated mobile ions is even further slower as they are now merely driven by ion diffusion without the electric field. Consequently, the dark recovery process occurs slowly. Therefore, the residue photocurrent, observed in the second round of light soaking (Time = 160 s of Figure 1(e)), can be explained by the mobile ions not yet recovered in the dark.

Mobile ions have a significant role in the working dynamics driven by light soaking.[50,51] It is also a consensus in the literature that these morphological domain boundaries of polycrystalline perovskite work as migration highway for these mobile ions[18,52]. Therefore, the engineering of perovskite morphological domain boundaries is often emphasized. However, in this study, it is observed that morphological domain distributions become indifferentiable in the FLIM images with cumulated light soaking, which is ascribed to the quenching of the PL intensity of the domain interiors (Figure 3). These observations bring attentions to the facts that in an operating PSC under working conditions, the impact of mobile ions/charge carriers would eventually apply on the whole perovskite films, and engineering of the planar defects and "crystallography grains"[53,54] in the perovskite morphological domain interiors are essential to improve the performance of PSCs.

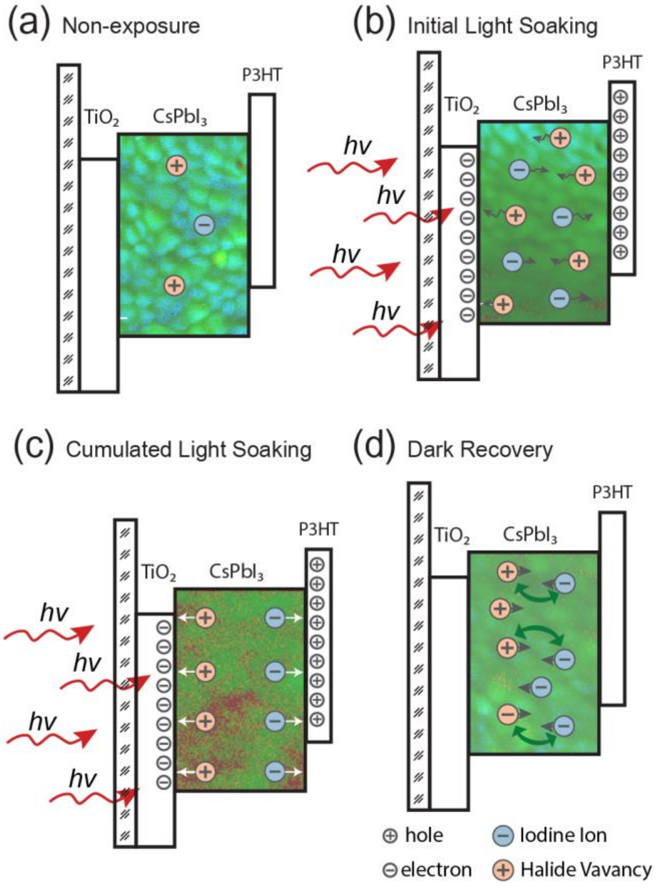

Figure 4. Illustration of charge carriers and mobile ion migration during light soaking and recovery processes.

In summary, using high resolution and high sensitivity FLIM, we have observed dynamic PL intensity and PL lifetime for operating perovskite solar cells during light soaking and recovery processes, which provided a deeper insight at perovskite/hole transport layer interface as well as grain interior and grain boundary of full-functional working solar cells. The changes in the solar cell photocurrent and voltage, together with the perovskite PL changes, are ascribed to the photogenerated internal electric field, which also drives the migration of mobiles ions. In contrast, the dark recovery after cumulated light soaking is relatively slow, driven only by reverse ions movement. While grain boundaries might be preferred by mobile ion migration, the bias-light-induced mobile ions affect the performance of the grain interiors, which must be considered when constituting device improvement strategies. Based on this understanding, alternative techniques could be generated to maximize and stabilize perovskite solar cells performance. Meanwhile, the characterization method developed based on FLIM to dynamically monitor the perovskite materials in a solar cell working condition is widely applicable to study other solar cells' performance with similar structures, providing detailed information on the photophysics of the materials.

ACKNOWLEDGMENT

B.J. and X.W. acknowledge support from the Australia Research Council through the Discovery Project scheme (DP190103186, DP190103284).

REFERENCES

(1) Kojima, A.; Teshima, K.; Shirai, Y.; Miyasaka, T. Organometal Halide Perovskites as Visible-Light Sensitizers for Photovoltaic Cells. *J. Am. Chem. Soc.* **2009**, *131* (17), 6050–6051.

(2) Best-Research-Cell-Efficiencies.20190703.Pdf.

(3) Yuan, M.; Quan, L. N.; Comin, R.; Walters, G.; Sabatini, R.; Voznyy, O.; Hoogland,

S.; Zhao, Y.; Beauregard, E. M.; Kanjanaboos, P. Perovskite Energy Funnels for Efficient Light-Emitting Diodes. *Nat. Nanotechnol.* **2016**, *11* (10), 872–877.

(4) Ahmadi, M.; Wu, T.; Hu, B. A Review on Organic-Inorganic Halide Perovskite Photodetectors: Device Engineering and Fundamental Physics. *Adv. Mater.* **2017**, *29* (41), 1605242.

(5) Fan, J.; Jia, B.; Gu, M. Perovskite-Based Low-Cost and High-Efficiency Hybrid Halide Solar Cells. *Photonics Res.* **2014**, *2* (5), 111.

(6) Eames, C.; Frost, J. M.; Barnes, P. R. F.; O'Regan, B. C.; Walsh, A.; Islam, M. S. Ionic Transport in Hybrid Lead Iodide Perovskite Solar Cells. *Nat. Commun.* **2015**, *6* (1), 7497.

(7) Chen, S.; Wen, X.; Sheng, R.; Huang, S.; Deng, X.; Green, M. A.; Ho-Baillie, A. Mobile Ion Induced Slow Carrier Dynamics in Organic–Inorganic Perovskite CH 3 NH 3 PbBr 3. *ACS Appl. Mater. Interfaces* **2016**, *8* (8), 5351–5357.

(8) Mosconi, E.; Meggiolaro, D.; Snaith, H. J.; Stranks, S. D.; De Angelis, F. Light-Induced Annihilation of Frenkel Defects in Organo-Lead Halide Perovskites. *Energy Environ. Sci.* **2016**, *9* (10), 3180–3187.

(9) Zheng, F.; Wen, X.; Bu, T.; Chen, S.; Yang, J.; Chen, W.; Huang, F.; Cheng, Y.-B.; Jia, B. Slow Response of Carrier Dynamics in Perovskite Interface upon Illumination. *ACS Appl. Mater. Interfaces* **2018**, *10*, acsami.8b13932.

(10) Zhao, C.; Chen, B.; Qiao, X.; Luan, L.; Lu, K.; Hu, B. Revealing Underlying Processes Involved in Light Soaking Effects and Hysteresis Phenomena in Perovskite Solar Cells. *Adv. Energy Mater.* **2015**, *5* (14), 1–6.

(11) Symonowicz, J.; Morawski, M.; Dusza, M.; Peksa, P.; Sieradzki, A.; Granek, F. Investigation of the Light-Soaking Effect in Organic Solar Cells Using Dielectric Permittivity and Electric Modulus Approaches. *Org. Electron. physics, Mater. Appl.* **2018**, *52* (July 2017), 32–41.

(12) Nie, W.; Blancon, J.-C.; Neukirch, A. J.; Appavoo, K.; Tsai, H.; Chhowalla, M.; Alam, M. A.; Sfeir, M. Y.; Katan, C.; Even, J.; et al. Light-Activated Photocurrent Degradation and Self-Healing in Perovskite Solar Cells. *Nat. Commun.* **2016**, *7* (May), 11574.

(13) Lau, C. F. J.; Deng, X.; Zheng, J.; Kim, J.; Zhang, Z.; Zhang, M.; Bing, J.; Wilkinson, B.; Hu, L.; Patterson, R.; et al. Enhanced Performance: Via Partial Lead Replacement with Calcium for a CsPbI3perovskite Solar Cell Exceeding 13% Power Conversion Efficiency. *J. Mater. Chem. A* **2018**, *6* (14), 5580–5586.

(14) Deng, X.; Wen, X.; Lau, J.; Young, T.; Yun, J.; Green, M.; Huang, S.; Ho-Baillie, A. W. Y. Electric Field Induced Reversible and Irreversible Photoluminescence Responses in Methylammonium Lead Iodide Perovskite. *J. Mater. Chem. C* **2016**, *4* (October), 9060–9068.

(15) Chen, S.; Wen, X.; Huang, S.; Huang, F.; Cheng, Y.; Green, M.; Ho-Baillie, A. Light Illumination Induced Photoluminescence Enhancement and Quenching in Lead Halide Perovskite. *Sol. RRL* **2017**, *1* (1), 1600001.

(16) Xing, G.; Mathews, N.; Lim, S. S.; Yantara, N.; Liu, X.; Sabba, D.; Grätzel, M.; Mhaisalkar, S.; Sum, T. C. Low-Temperature Solution-Processed Wavelength-Tunable Perovskites for Lasing. *Nat. Mater.* **2014**, *13* (5), 476–480.

(17) Xiao, Z.; Yuan, Y.; Shao, Y.; Wang, Q.; Dong, Q.; Bi, C.; Sharma, P.; Gruverman, A.;

Huang, J. Giant Switchable Photovoltaic Effect in Organometal Trihalide Perovskite Devices. *Nat. Mater.* **2015**, *14* (2), 193–197.

(18) Li, W.; Rothmann, M. U.; Liu, A.; Wang, Z.; Zhang, Y.; Pascoe, A. R.; Lu, J.; Jiang, L.; Chen, Y.; Huang, F.; et al. Phase Segregation Enhanced Ion Movement in Efficient Inorganic CsPbIBr 2 Solar Cells. *Adv. Energy Mater.* **2017**, *1700946*, 1700946.

(19) Muscarella, L. A.; Hutter, E. M.; Sanchez, S.; Dieleman, C. D.; Savenije, T. J.; Hagfeldt, A.; Saliba, M.; Ehrler, B. Crystal Orientation and Grain Size: Do They Determine Optoelectronic Properties of MAPbI3 Perovskite? *J. Phys. Chem. Lett.* **2019**, *10* (20), 6010–6018.

(20) Wen, X.; Sheng, R.; Ho-Baillie, A. W. Y.; Benda, A.; Woo, S.; Ma, Q.; Huang, S.; Green, M. A. Morphology and Carrier Extraction Study of Organic–Inorganic Metal Halide Perovskite by One- and Two-Photon Fluorescence Microscopy. *J. Phys. Chem. Lett.* **2014**, *5* (21), 3849–3853.

(21) de Quilettes, D. W.; Vorpahl, S. M.; Stranks, S. D.; Nagaoka, H.; Eperon, G. E.; Ziffer, M. E.; Snaith, H. J.; Ginger, D. S. Impact of Microstructure on Local Carrier Lifetime in Perovskite Solar Cells. *Science (80-.).* **2015**, *348* (6235), 683–686.

(22) Zheng, F.; Chen, W.; Bu, T.; Ghiggino, K. P.; Huang, F.; Cheng, Y.; Tapping, P.; Kee, T. W.; Jia, B.; Wen, X. Triggering the Passivation Effect of Potassium Doping in Mixed-Cation Mixed-Halide Perovskite by Light Illumination. *Adv. Energy Mater.* **2019**, *1901016*, 1–11.

(23) Wen, X.; Huang, S.; Chen, S.; Deng, X.; Huang, F.; Cheng, Y.; Green, M.; Ho-Baillie, A. Optical Probe Ion and Carrier Dynamics at the CH 3 NH 3 PbI 3 Interface with Electron and Hole Transport Materials. *Adv. Mater. Interfaces* **2016**, *3* (22), 1600467.

(24) Zhang, J.; Daniel, Q.; Zhang, T.; Wen, X.; Xu, B.; Sun, L.; Bach, U.; Cheng, Y. B. Chemical Dopant Engineering in Hole Transport Layers for Efficient Perovskite Solar Cells: Insight into the Interfacial Recombination. *ACS Nano* **2018**.

(25) Chen, W.; Mao, W.; Bach, U.; Jia, B.; Wen, X. Tracking Dynamic Phase Segregation in Mixed-Halide Perovskite Single Crystals under Two-Photon Scanning Laser Illumination. *Small Methods* **2019**, *3*, 1900273.

(26) Sheng, R.; Wen, X.; Huang, S.; Hao, X.; Chen, S.; Jiang, Y.; Deng, X.; Green, M. A.; Ho-Baillie, A. W. Y. Photoluminescence Characterisations of a Dynamic Aging Process of Organic-Inorganic CH3NH3PbBr3 Perovskite. *Nanoscale* **2016**, *8* (4), 1926–1931.

(27) Chen, W.; Wen, X.; Yang, J.; Latzel, M.; Patterson, R.; Huang, S.; Shrestha, S.; Jia, B.; Moss, D. J.; Christiansen, S.; et al. Free Charges versus Excitons: Photoluminescence Investigation of InGaN/GaN Multiple Quantum Well Nanorods and Their Planar Counterparts. *Nanoscale* **2018**, *10* (11), 5358–5365.

(28) Chen, W.; Wen, X.; Latzel, M.; Heilmann, M.; Yang, J.; Dai, X.; Huang, S.; Shrestha, S.; Patterson, R.; Christiansen, S. Nanoscale Characterization of Carrier Dynamic and Surface Passivation in InGaN/GaN Multiple Quantum Wells on GaN Nanorods. *ACS Appl. Mater. Interfaces* **2016**, *8* (46), 31887–31893.

(29) Li, C.; Guerrero, A.; Huettner, S.; Bisquert, J. Unravelling the Role of Vacancies in Lead Halide Perovskite through Electrical Switching of Photoluminescence. *Nat. Commun.* **2018**, *9* (1).

(30) Abdi-Jalebi, M.; Andaji-Garmaroudi, Z.; Cacovich, S.; Stavrakas, C.; Philippe, B.; Richter, J. M.; Alsari, M.; Booker, E. P.; Hutter, E. M.; Pearson, A. J.; et al.

Maximizing and Stabilizing Luminescence from Halide Perovskites with Potassium Passivation. *Nature* **2018**, *555* (7697), 497–501.

(31) Akin, S.; Arora, N.; Zakeeruddin, S. M.; Grätzel, M.; Friend, R. H.; Dar, M. I. New Strategies for Defect Passivation in High-Efficiency Perovskite Solar Cells. *Adv. Energy Mater.* **2019**, *2*, 1–29.

(32) Zhong, Y.; Luna, C. A. M.; Hildner, R.; Li, C.; Huettner, S. In Situ Investigation of Light Soaking in Organolead Halide Perovskite Films. *APL Mater.* **2019**, *7* (4).

(33) Ruan, S.; Surmiak, M. A.; Ruan, Y.; McMeekin, D. P.; Ebendorff-Heidepriem, H.; Cheng, Y. B.; Lu, J.; McNeill, C. R. Light Induced Degradation in Mixed-Halide Perovskites. *J. Mater. Chem. C* **2019**, *7* (30), 9326–9334.

(34) Wen, X.; Feng, Y.; Huang, S.; Huang, F.; Cheng, Y.-B.; Green, M.; Ho-Baillie, A. Defect Trapping States and Charge Carrier Recombination in Organic–Inorganic Halide Perovskites. *J. Mater. Chem. C* **2016**, *4* (4), 793–800.

(35) Stranks, S. D.; Burlakov, V. M.; Leijtens, T.; Ball, J. M.; Goriely, A.; Snaith, H. J. Recombination Kinetics in Organic-Inorganic Perovskites: Excitons, Free Charge, and Subgap States. *Phys. Rev. Appl.* **2014**, *2* (3), 1–8.

(36) Xing, G.; Mathews, N.; Sun, S.; Lim, S. S.; Lam, Y. M.; Grätzel, M.; Mhaisalkar, S.; Sum, T. C. Long-Range Balanced Electron-and Hole-Transport Lengths in Organic-Inorganic CH3NH3PbI3. *Science.* **2013**, *342* (6156), 344–347.

(37) Yuan, Y.; Huang, J. Ion Migration in Organometal Trihalide Perovskite and Its Impact on Photovoltaic Efficiency and Stability. *Acc. Chem. Res.* **2016**, *49*, 286–293.

(38) Calado, P.; Telford, A. M.; Bryant, D.; Li, X.; Nelson, J.; O'Regan, B. C.; Barnes, P.

R. F. Evidence for Ion Migration in Hybrid Perovskite Solar Cells with Minimal Hysteresis. *Nat. Commun.* **2016**, *7*, 13831.

(39) Richardson, G.; O'Kane, S. E. J.; Niemann, R. G.; Peltola, T. A.; Foster, J. M.; Cameron, P. J.; Walker, A. B. Can Slow-Moving Ions Explain Hysteresis in the Current-Voltage Curves of Perovskite Solar Cells? *Energy Environ. Sci.* **2016**, *9* (4), 1476–1485.

(40) Azpiroz, J. M.; Mosconi, E.; Bisquert, J.; De Angelis, F. Defect Migration in Methylammonium Lead Iodide and Its Role in Perovskite Solar Cell Operation. *Energy Environ. Sci.* **2015**, *8* (7), 2118–2127.

(41) Pockett, A.; Carnie, M. J. Ionic Influences on Recombination in Perovskite Solar Cells. *ACS Energy Lett.* **2017**, *2* (7), 1683–1689.

(42) Brennan, M. C.; Draguta, S.; Kamat, P. V.; Kuno, M. Light-Induced Anion Phase Segregation in Mixed Halide Perovskites. *ACS Energy Lett.* **2018**, *3* (1), 204–213.

(43) Tress, W.; Marinova, N.; Moehl, T.; Zakeeruddin, S. M.; Nazeeruddin, M. K.; Grätzel, M. Understanding the Rate-Dependent J-V Hysteresis, Slow Time Component, and Aging in CH 3 NH 3 PbI 3 Perovskite Solar Cells: The Role of a Compensated Electric Field. *Energy Environ. Sci.* **2015**, *8* (3), 995–1004.

(44) Lopez-Varo, P.; Jiménez-Tejada, J. A.; García-Rosell, M.; Anta, J. A.; Ravishankar, S.; Bou, A.; Bisquert, J. Effects of Ion Distributions on Charge Collection in Perovskite Solar Cells. *ACS Energy Lett.* **2017**, *2* (6), 1450–1453.

(45) Yang, J.; Wen, X.; Xia, H.; Sheng, R.; Ma, Q.; Kim, J.; Tapping, P.; Harada, T.; Kee, T. W.; Huang, F.; et al. Acoustic-Optical Phonon up-Conversion and Hot-Phonon Bottleneck in Lead-Halide Perovskites. *Nat. Commun.* **2017**, *8* (1), 14120.

(46) Walsh, A.; Stranks, S. D. Taking Control of Ion Transport in Halide Perovskite Solar Cells. *ACS Energy Lett.* **2018**, 1983–1990.

(47) Bischak, C. G.; Wong, A. B.; Lin, E.; Limmer, D. T.; Yang, P.; Ginsberg, N. S. Tunable Polaron Distortions Control the Extent of Halide Demixing in Lead Halide Perovskites. *J. Phys. Chem. Lett.* **2018**, *9* (14), 3998–4005.

(48) Bischak, C. G.; Hetherington, C. L.; Wu, H.; Aloni, S.; Ogletree, D. F.; Limmer, D. T.; Ginsberg, N. S. Origin of Reversible Photoinduced Phase Separation in Hybrid Perovskites. *Nano Lett.* **2017**, *17* (2), 1028–1033.

(49) Kim, G. Y.; Senocrate, A.; Yang, T. Y.; Gregori, G.; Grätzel, M.; Maier, J. Large Tunable Photoeffect on Ion Conduction in Halide Perovskites and Implications for Photodecomposition. *Nat. Mater.* **2018**, *17* (5), 445–449.

(50) Huang, F.; Jiang, L.; Pascoe, A. R.; Yan, Y.; Bach, U.; Spiccia, L.; Cheng, Y.-B. Fatigue Behavior of Planar CH 3 NH 3 PbI 3 Perovskite Solar Cells Revealed by Light on/off Diurnal Cycling. *Nano Energy* **2016**, *27*, 509–514.

(51) Jiang, L.; Lu, J.; Raga, S. R.; Sun, J.; Lin, X.; Huang, W.; Huang, F.; Bach, U.; Cheng, Y. B. Fatigue Stability of CH 3 NH 3 PbI 3 Based Perovskite Solar Cells in Day/Night Cycling. *Nano Energy* **2019**, *58* (February), 687–694.

(52) Shao, Y.; Fang, Y.; Li, T.; Wang, Q.; Dong, Q.; Deng, Y.; Yuan, Y.; Wei, H.; Wang, M.; Gruverman, A.; et al. Grain Boundary Dominated Ion Migration in Polycrystalline Organic–Inorganic Halide Perovskite Films. *Energy Environ. Sci.* **2016**, *9* (5), 1752–1759.

(53) Jariwala, S.; Sun, H.; Adhyaksa, G. W. P.; Lof, A.; Muscarella, L. A.; Ehrler, B.; Garnett, E. C.; Ginger, D. S. Local Crystal Misorientation Influences Non-Radiative

Recombination in Halide Perovskites. *Joule* **2019**, 1–13.

(54) Li, W.; Yadavalli, S. K.; Lizarazo-Ferro, D.; Chen, M.; Zhou, Y.; Padture, N. P.; Zia, R. Subgrain Special Boundaries in Halide Perovskite Thin Films Restrict Carrier Diffusion. *ACS Energy Lett.* **2018**, *3* (11), 2669–2670.